Jiawen Li, Erik Schartner, Stefan Musolino, Bryden C. Quirk, Rodney W. Kirk, Heike Ebendorff-Heidepriem and Robert A. McLaughlin

Miniaturized single-fiber-based needle probe for combined imaging and sensing in deep tissue

Optics Letters, 2018; 43(8):1682-1685

Published version: http://dx.doi.org/10.1364/OL.43.001682

Miniaturized single-fiber-based needle probe for combined imaging and sensing in deep tissue

JIAWEN LI[1,2,3,*], ERIK SCHARTNER[1,2,4], STEFAN MUSOLINO[1,2,3], BRYDEN C. QUIRK[1,2,3], RODNEY W. KIRK[1,2,3], HEIKE EBENDORFF-HEIDEPRIEM[1,2,4], ROBERT A. MCLAUGHLIN[1,2,3]

[1]*Australian Research Council Centre of Excellence for Nanoscale BioPhotonics, University of Adelaide, Adelaide, Australia*
[2]*Institute for Photonics and Advanced Sensing, University of Adelaide, Adelaide, Australia*
[3]*Adelaide Medical School, The University of Adelaide, Adelaide, Australia*
[4]*School of Physical Sciences, The University of Adelaide, Adelaide, Australia*
**Corresponding author: jiawen.li01@adelaide.edu.au*

Received XX Month XXXX; revised XX Month, XXXX; accepted XX Month XXXX; posted XX Month XXXX (Doc. ID XXXXX); published XX Month XXXX

The ability to visualize structure whilst simultaneously measuring chemical or physical properties of a biological tissue has the potential to improve our understanding of complex biological processes. We report the first miniaturized single-fiber-based imaging+sensing probe capable of simultaneous optical coherence tomography (OCT) imaging and temperature sensing. An OCT lens is fabricated at the distal end of a double clad fiber, including a thin layer of rare-earth doped tellurite glass to enable temperature measurements. The high refractive index of the tellurite glass enables a common-path interferometer configuration for OCT, allowing easy exchange of probes for biomedical applications. The simultaneous imaging+sensing capability is demonstrated on rat brains. © 2017 Optical Society of America

OCIS codes: *(170.0170) Medical optics and biotechnology; (060.2370) Fiber optics sensors; (060.2350) Fiber optics imaging; (170.4500) Optical coherence tomography; (280.4788) Optical sensing and sensor.*

http://dx.doi.org/10.1364/OL.99.099999

Miniaturized fiber-optic imaging probes, such as those based on optical coherence tomography (OCT), enable us to image deep inside the body with micron-scale resolution, and have demonstrated utility in a wide range of biomedical applications [1, 2]. However, these OCT fiber imaging probes are limited to acquiring structural information, and lack the capability to sense functional information that would be desirable for advancing the fundamental understanding of complex biological processes [3-5]. In parallel, a wide range of optical sensing techniques have been developed in non-imaging applications, providing insight into physiologically important parameters such as temperature [4], pH [5], metal ions [3], hydrogen peroxide [6] or other small molecules [7]. However, current fiber sensing approaches do not provide information about the local tissue structure, rendering them subject to measurement artifacts because of structural heterogeneity or misplacement of the fiber sensing probe. For example, previous work has demonstrated a portable configuration of a fiber-optic sensing probe to monitor local temperature changes in rat brains [4], with the probe inserted into an anatomical region of interest (ROI) relative to a standardized rat brain atlas. This semi-blind procedure is done without intraoperative imaging guidance and is subject to inter-subject variations due to anatomical differences between animals [8]. In this paper, we propose a novel multi-modal imaging+sensing fiber-optic probe that provides additional insight over imaging alone and mitigates many potential measurement artifacts present in unguided sensing.

Earlier work has demonstrated integrated OCT+fluorescence fiber-optic probes [9-12]. Cell-specific or disease-specific fluorophores are introduced for specific labeling of tissue, providing molecular contrast. We build upon this work, but utilize the fluorescence signal for fluorescence-based fiber sensing by incorporating a functionalized fluorescent coating on the distal tip of the fiber [13, 14]. These sensing approaches can be utilized to detect the presence of specific molecules [6, 7], as well as a wide range of physiological parameters, such as temperature and ion concentration [3-5].

In a previous example of imaging+sensing, Michael et al. [14] made a fiber bundle-based imaging probe, comprising several thousand fiber cores, and coated with a pH-sensitive film. The device enabled reflectance microscopy imaging and sensing for acid release during fertilization of eggs. The technique demonstrated the potential of such a combined approach, but lacked the depth differentiation of tissue that is possible by utilizing an OCT probe as the imaging component.

Here we have developed, for the first time, a single-fiber-based imaging+sensing probe that can provide co-localized OCT tissue visualization and measurement of temperature, in deep tissue. We describe the design and fabrication of the imaging+sensing probe and demonstrate its performance on *ex vivo* rat brain samples.

The fabrication of the sensing and imaging elements used here has been previously explored as two distinct probes [14, 15], with these being combined here into a single, multi-functional probe. As shown in Fig. 1 (a), the probe consists of a 35 cm length of double-clad fiber (DCF, with a 125 µm cladding diameter, DCF13, Thorlabs Inc., USA), terminated with a microlens to focus the OCT light beam that is transmitted through the core of the DCF. The microlens is constructed by splicing 190 µm of no-core fiber (NCF, 125 µm cladding diameter, POFC, Taiwan) to the distal end of the DCF, to expand the OCT light beam from the core. This was then dipped in a rare-earth doped tellurite glass melt to form a curved, focusing element terminating the fiber, as shown in Fig 1(b). Using microscopic images of the distal tip of the fiber, we manually measured the radius of the focusing element of 4 probes, to be 78±1 µm. To fabricate reproducible optics, we found it important to control for temperature of the glass melt (815°C) and time between removing the glass melt from the oven and performing the dip-coating (5 s) [16]. The output beam from the probe has a working distance of 335 µm in water (146 µm in air due to the larger refractive index difference between air and tellurite). The beam profile, shown in Fig 1(c), was measured in air with a CMOS camera-based beam profiler (WinCamD-XHR-1310, DataRay Inc., USA) using an OCT light source (SLD1325, Thorlabs Inc., USA). The simulation result was obtained by setting the radius of curvature for the tellurite portion of the probe as 78 µm and the thickness as 40 µm, which are averaged values measured across 4 probes. To increase the robustness of the fiber probe and avoid breakage during animal experiments, the optical assembly was protected inside a modified 25-gauge needle (outer diameter 520 µm) [4], leaving approximately 2 mm of bare fiber protruded from the distal end of the needle for sensing.

Temperature sensitivity is incorporated into the probe through dipping the end of the assembled OCT probe into a molten glass doped with erbium and ytterbium, using a method reported previously for standard single mode fibers [14]. The populations of two thermally linked energy states of the erbium ions change depending on the environmental temperature, with the temperature then determined by monitoring the ratio of two emission bands (524 nm and 547 nm), which is insensitive to fluctuations of the excitation intensity [17, 18]. This rare-earth thermometry technique utilizes upconversion as the pumping mechanism, using a near infrared source that minimizes autofluorescence emissions typically seen in biological samples [14].

For this project, tellurite glass was used for the fabrication of the temperature sensitive region, as it has low phonon energy, and can accommodate the high rare earth doping concentrations that allows for efficient upconversion generation [19]. Additionally, it possesses the low melting temperature (815 °C) required to avoid deformation of the silica glass during the dipping process, and has a high refractive index to increase the backreflection at the fiber/tellurite interface that is used to generate a common-path OCT signal [14]. This common-path configuration has the advantage of minimizing issues of dispersion or polarization mismatch, often seen in dual-arm OCT configurations, and

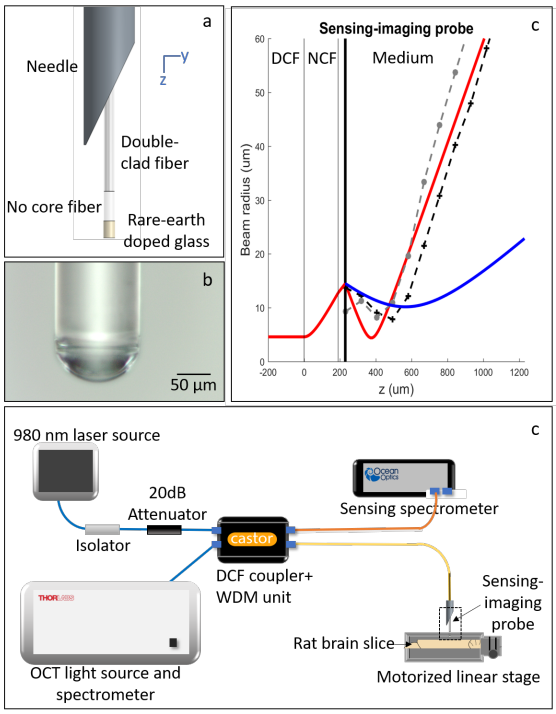

Figure 1 (a) Schematic design of the tip of the imaging+sensing probe; (b) microscopic photo of the tip of the probe, showing the curved tellurite focusing element (c) simulated and measured beam diameters of the imaging+sensing probe; (d) schematic of the entire system. In (c), solid black vertical line denotes the interface between tellurite and the external medium (air or water); red and blue curves represent the simulated beam propagation in air and in water respectively; black and grey dotted curves represent the measured beam diameters in x and y axes, respectively, which were obtained in air; z: physical distance; DCF: double-clad fiber; NCF: no core fiber. In (d), note the dashed box drawn around the imaging probe in the bottom right. This corresponds to the zoomed schematic view shown in (a). Blue line: single mode fiber; orange line: multimode fiber; light orange line: double-clad fiber

avoiding the need to carefully match the optical pathlengths of separate sample and reference arms. In practice, this allows quick and easy interchange of the imaging+sensing probes during experiments.

The integrated system is shown in Fig. 1 (c). In the sensing sub-system, a compact 980 nm laser (BF-970-0300, Thorlabs, USA) and a portable spectrometer (QE65 Pro, Ocean Optics, USA) were used for excitation of the doped fiber tips, and to spectrally analyze the up-conversion emission for temperature measurement, respectively. Due to the strong fluorescence signal that can be collected via the probe, the laser was attenuated by 20 dB, with a transmitted power through the probe of less than 0.5 mW. To minimize backscattered 980 nm pump incident on the spectrometer, a dichroic-coated collection filter (800 nm SP, Omega Filters, USA) was used to avoid the need for bulk optics seen in previous work [4]. In the imaging sub-system, the light source (nominal wavelength: 1300 nm) and the spectrometer of a commercially-available OCT system (Telesto III, Thorlabs, USA) were utilized. The exposure time to obtain each A-scan was set as 13.1 µs during tissue experiments. These two subsystems were

integrated using a customized DCF coupler module (Castor Optics, Canada), comprising a wavelength division multiplexer (WDM) and a double-clad fiber coupler (DCFC). In the DCF-based dual-function probe, the single mode core of the DCF carries the OCT signal to and from the sample, and also the fluorescence excitation light for temperature sensing. Emitted fluorescence is collected within the inner cladding of the DCF. The WDM combines the OCT light and the 980 nm laser source, while DCFC separates the detected signals in the core (for imaging) and inner cladding (for sensing), and couples them into the OCT system and sensing spectrometer, respectively.

A temperature calibration plot for the probe was obtained by placing it in a water bath with a resistance temperature detector (RTD, 100 Ω Class A, Omega Engineering, USA) positioned within 1 mm of the probe [4]. Custom LabView software was used to simultaneously record the reference temperature obtained by the RTD and the emission spectra from the probe. The emission spectra were then used to calculate fluorescence ratios at two wavelength bands as described in [3], generating a calibration curve modeled with a second order polynomial (R^2=0.999). A small change in the observed fluorescence ratio was seen if the OCT source was turned on or off, and as a result all temperature measurements were performed with the OCT scans running.

To demonstrate usage of the probe for simultaneous temperature sensing and imaging within tissue, we conducted an experiment in an intact, *ex vivo* rat brain. To test across the range of biologically relevant temperatures, the brain and RTD were submerged in a warm water bath and slowly cooled to room temperature (Fig. 2(b)). As the probe was inserted into the rat brain, motion-mode (M-mode) images of OCT A-scans versus time, and temperature measurements were obtained concurrently. Fig. 2(c) is an M-mode image recorded as the tip of the probe penetrates the rat brain, allowing visualization of vessel structures before entering a region of highly scattering, solid tissue. Fig. 2(d) shows temperature readings, extending from initial insertion until the brain had cooled to room temperature. The time point at which Fig. 2(c) was acquired is indicated by the vertical red line on Fig. 2(d). Once the probe had been positioned at the ROI, no notable change was observed in the OCT M-mode image.

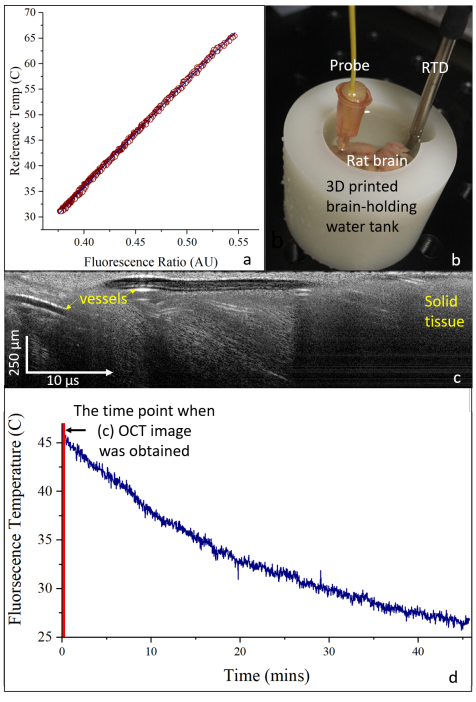

Figure 2 (a) Fluorescence ratio vs. reference temperature for increasing temperature, R^2 =0.999; (b) Photo showing the setup for *ex vivo* rat brain experiment; (c) M-mode structural OCT image during probe insertion; (d) Rat brain temperature measurements obtained by the imaging+sensing probe. The red vertical line in (d) indicates when the OCT image (c) was obtained.

To assess the imaging+sensing probe's capability to differentiate brain tissue types and provide image guidance, we imaged a dissected rat brain, mounting the probe on a 2D linear stage and scanning it over the tissue sample as shown in Fig. 1(c). This setup allowed us to obtain co-registered histology for validation of structures visualized in the OCT. Fig. 3 shows a representative *en face* OCT image with matching hematoxylin and eosin (H&E) histology. The striated appearance of the dark-and-bright region indicated the location of the striatum. Anterior commissure, which comprises a bundle of nerve fibers (white matter), appeared as a large oval-shaped region of low back scatter (dark grey) in the OCT image, and is clearly differentiated from the surrounding septal area.

In this paper, we have presented a forward-facing imaging probe. Such a probe has the potential to allow tissue differentiation mechanisms such as estimation of the attenuation coefficient [20-22] and differentiation of solid tissue from blood vessels through speckle decorrelation [23]. However, side-viewing configurations are also possible, enabling the acquisition of a B-scan on insertion of the probe, and providing visualization of tissue microstructure. Such a configuration can be realized by terminating the no-core fiber in the focusing optics with an angle-polished and metal-coated surface, such as that presented by Lorenser et al. [24].

In addition to temperature sensing, the imaging+sensing probe design reported in this study has the potential to be utilized with a range of other fluorescence-based sensing techniques, particularly those that are realized by a single-fiber-based tip sensor design [5, 6, 13].

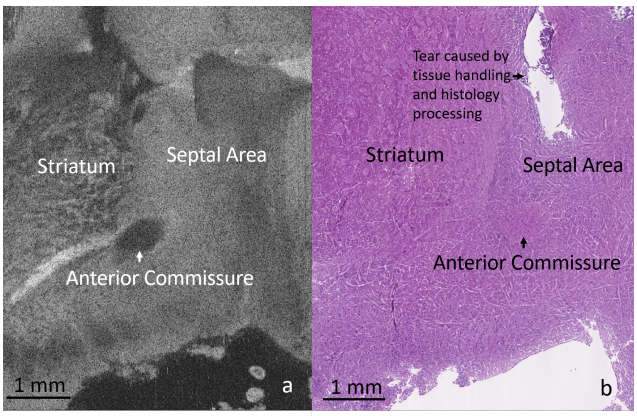

Figure 3 (a) En-face OCT image obtained in a rat brain. Visible structures include the striatum, anterior commissure and septal area, consistent with (b), which show co-located H&E histology.

In conclusion, we have demonstrated the first single-fiber-based OCT imaging+sensing probe. This probe can simultaneously image tissue microarchitecture and measure local temperature. The design not only enables the precise placement of fiber sensors, but also provides structural information to complement the functional measurements of the fiber sensor. Incorporating this combined probe into a needle enabled measurements to be acquired in deep tissue, well beyond the depth penetration of a superficial optical signal. Measurements in rat brains demonstrated the practical use of this novel probe in a biological sample.

Funding. The University of Adelaide (Institute for Photonics and Advanced Sensing 2017 pilot project); Australian Research Council (CE140100003, LP110200736, and DP150104660); and a Premier's Research and Industry Fund grant provided by the South Australian Government Department of State Development.

Acknowledgment. We would like to thank Prof. Mark Hutchinson and Ms. Vicky Staikopoulos for their technical support in rat brain atlas, and Ms. Kathryn Batra for her assistance in histology processing. The authors would like to also acknowledge Castor Optics for spending time and efforts in customizing the DCF coupler+WDM unit. This work was performed in part at the OptoFab node of the Australian National Fabrication Facility utilizing Australian Commonwealth and South Australian State Government funding.

References

1. E. A. Swanson and J. G. Fujimoto, Biomed. Opt. Express 8, 1638-1664 (2017).
2. M. J. Gora, M. J. Suter, G. J. Tearney, and X. Li, Biomed. Opt. Express 8, 2405-2444 (2017).
3. G. Cui, S. B. Jun, X. Jin, G. Luo, M. D. Pham, D. M. Lovinger, S. S. Vogel, and R. M. Costa, Nat. Protoc. 9, 1213 (2014).
4. S. Musolino, E. P. Schartner, G. Tsiminis, A. Salem, T. M. Monro, and M. R. Hutchinson, Biomed. Opt. Express 7, 3069-3077 (2016).
5. E. P. Schartner, M. R. Henderson, M. Purdey, D. Dhatrak, T. M. Monro, P. G. Gill, and D. F. Callen, Cancer Res. 76, 6795-6801 (2016).
6. M. S. Purdey, J. G. Thompson, T. M. Monro, A. D. Abell, and E. P. Schartner, Sensors 15, 31904-31913 (2015).
7. X.-d. Wang and O. S. Wolfbeis, Anal. Chem. 88, 203-227 (2015).
8. N. Kovačević, J. T. Henderson, E. Chan, N. Lifshitz, J. Bishop, A. C. Evans, R. M. Henkelman, and X. J. Chen, Cereb. Cortex 15, 639-645 (2004).
9. H. Yoo, J. W. Kim, M. Shishkov, E. Namati, T. Morse, R. Shubochkin, J. R. McCarthy, V. Ntziachristos, B. E. Bouma, F. A. Jaffer, and G. J. Tearney, Nat. Med. 17, 1680-1684 (2011).
10. S. Liang, A. Saidi, J. Jing, G. Liu, J. Li, J. Zhang, C. Sun, J. Narula, and Z. Chen, J. Biomed. Opt. 17, 0705011-0705013 (2012).
11. L. Scolaro, D. Lorenser, W.-J. Madore, R. W. Kirk, A. S. Kramer, G. C. Yeoh, N. Godbout, D. D. Sampson, C. Boudoux, and R. A. McLaughlin, B Biomed. Opt. Express 6, 1767-1781 (2015).
12. H. Pahlevaninezhad, A. M. D. Lee, G. Hohert, S. Lam, T. Shaipanich, E.-L. Beaudoin, C. MacAulay, C. Boudoux, and P. Lane, Opt. Lett. 41, 3209-3212 (2016).
13. W. Tan, Z.-Y. Shi, S. Smith, D. Birnbaum, and R. Kopelman, Science 258, 778-782 (1992).
14. E. P. Schartner and T. M. Monro, Sensors 14, 21693-21701 (2014).
15. R. A. McLaughlin, D. Lorenser, and D. D. Sampson, in Handbook of Coherent-Domain Optical Methods (Springer, 2013), pp. 1065-1102.
16. N. M. Parikh, J. Am. Ceram. Soc. 41, 18-22 (1958).
17. S. A. Wade, J. C. Muscat, S. F. Collins, and G. W. Baxter, Rev. Sci. Instrum. 70, 4279-4282 (1999).
18. V. Kumar Rai, Appl. Phys. B 88(2007).
19. F. Vetrone, J.-C. Boyer, J. A. Capobianco, A. Speghini, and M. Bettinelli, Appl. Phys Lett. 80, 1752-1754 (2002).
20. R. A. McLaughlin, L. Scolaro, P. Robbins, C. Saunders, S. L. Jacques, and D. D. Sampson, J. Biomed. Opt. 15, 046029 (2010).
21. C. Xu, J. M. Schmitt, S. G. Carlier, and R. Virmani, J. Biomed. Opt. 13, 034003 (2008).
22. F. J. van der Meer, D. J. Faber, D. M. B. Sassoon, M. C. Aalders, G. Pasterkamp, and T. G. van Leeuwen, IEEE Trans. Med. Imag. 24, 1369-1376 (2005).
23. N. Uribe-Patarroyo, M. Villiger, and B. E. Bouma, Opt. Express 22, 24411-24429 (2014).
24. D. Lorenser, X. Yang, R. W. Kirk, B. C. Quirk, R. A. McLaughlin, and D. D. Sampson, Opt. Lett. 36, 3894-3896 (2011).